



RESEARCH ARTICLE

Enhanced Performance of Fabricated Iodine-Rich Perovskite Solar Cells via Reverse-Biasing

Yingfeng Li | Zixuan Wang | Peici Yu | Yuewen Chen | Rongxin Wu | Xing Zhao | Peng Cui | Hao Huang | Meicheng Li

State Key Laboratory of Alternate Electrical Power System with Renewable, Energy Sources, School of New Energy, North China Electric Power University, Beijing, China

Correspondence: Meicheng Li (mcli@ncepu.edu.cn)

Received: 26 January 2025 | **Revised:** 26 March 2025 | **Accepted:** 31 March 2025

Funding: National Natural Science Foundation of China, Grant/Award Numbers: 52072121 52232008 51972110 52102245 52402254 22409061; Beijing Natural Science Foundation, Grant/Award Numbers: Z240024 2222076 2222077; 2022 Strategic Research Key Project of Science and Technology Commission of the Ministry of Education, Huaneng Group Headquarters Science and Technology Project, Grant/Award Number: HNKJ20-H88; State Key Laboratory of Alternate Electrical Power System with Renewable Energy Sources, Grant/Award Number: LAPS2024-05; Fundamental Research Funds for the Central Universities, Grant/Award Numbers: 2022MS029 2022MS02 2022MS031 2023MS042 2023MS047; “NCEPU “Double First-Class” Program

Keywords: iodine-rich | perovskite solar cells | reverse-biasing | short-circuit current

ABSTRACT

Perovskite solar cells (PSCs) are undergoing rapid development and exhibit considerable potential for commercialization. Recent studies have shown that reverse bias can improve the open-circuit voltage (V_{OC}) of PSCs by ≈ 0.06 V due to the migration of iodine ions filling vacancies at the electron transport layer (ETL)/perovskite interface. It can be deduced that in iodine-rich PSCs, the potential for reverse-biasing to enhance V_{OC} is limited due to the suppression of iodine vacancies by excess iodine atoms. This work confirms that, in iodine-rich PSCs, reverse bias has a minimal effect on V_{OC} , but leads to a $\approx 3.9\%$ increase in short-circuit current density (J_{SC}), from 25.40 to 26.40 mA/cm², and an enhancement of $\approx 3.2\%$ in power conversion efficiency from 23.00% to 23.74%. The improved J_{SC} can be attributed to reduced carrier recombination near the ETL/perovskite interface, as evidenced by enhanced external quantum efficiency and increased recombination resistance in the short-wavelength region. These insights suggest a practical posttreatment strategy for high-performance PSCs.

1 | Introduction

Organic–inorganic hybrid perovskite solar cells (PSCs) have experienced rapid development, with the certified highest power conversion efficiency (PCE) reaching 26.7% [1, 2]. Various strategies have been developed to enhance the PCE of PSCs, including interface passivation technologies [3–6], improving the crystallization quality of the perovskite layer [7–10], and enhancing the built-in electric field [11]. For instance, Wang et al. developed an in situ dual-interface passivation strategy to mitigate deep interface defects, leading to an approximately 12% increase in PCE [3]. Yang et al. achieved record-efficiency flexible PSCs by synthesizing a multifunctional organic ion to passivate the electron transport layer (ETL)/perovskite

interface [4]. Zhao et al. demonstrated that citric acid can eliminate the PbI₂-DMSO complexes located at the buried perovskite interface, which not only increases the perovskite crystal size but also effectively suppresses nonradiative recombination at the interface, resulting in a PCE enhancement of $\approx 3.7\%$ [5]. Recently, Zhang et al. proposed a universal ternary solvent system composed of tetrahydrothiophene 1-oxide, chlorobenzene, and isopropanol to improve the perovskite surface passivation effects, which is universal for different passivators and perovskite films with various compositions, impressively leading to the PCE of PSCs exceed 26% [6]. Wu et al. reported that the perovskite crystallization can be effectively modulated using the organic small molecule (6BAS) as an additive, resulting in a 10.5% increase in PCE [9]. Cui et al. constructed a novel p–n homojunction

Yingfeng Li and Meicheng Li contributed equally to this work.

© 2025 Wiley-VCH GmbH.

perovskite solar cell which promoted oriented transport of carriers, thus reducing carrier recombination losses [11].

Recently, Huang et al. revealed that reverse bias can enhance the open-circuit voltage (V_{OC}) of PSCs from 1.10 V to 1.16 V [12]. They demonstrated that during reverse bias, the migration of iodine ions toward the ETL/perovskite interface facilitates the filling of iodine vacancies, thereby augmenting the built-in electric field, which leads to an increase in PCE from 22.13% to 23.48%. And, Meng et al. reported an approximate 4.2% enhancement in the efficiency of PSCs during maximum power point stability assessments following the application of bias voltage treatment [13]. This improvement is ascribed to the mitigation of cell defects resulting from ion migration induced by the electric field. In addition, Jeong K et al. found that reverse bias can recover power degradation and enhance the stability of PSCs [14]. This is because reverse bias pulse can facilitate the redistribution of ions and the repair of defects in the perovskite layer. However, it has been observed that under conditions of high and sustained reverse bias voltage, the performance of PSCs experiences a significant decline [15–17]. For instance, Fei et al. demonstrated that after 2 min of continuous reverse bias at -1 V, ion migration damages the crystal structure of the perovskite, leading to a 52.3% decrease in the PCE of MAPbI₃ devices [15]. Given the limited existing research on improving device performance through reverse bias, further studies are essential to explore its impacts on the performance enhancement of various types of PSCs.

Many studies have demonstrated that iodine-rich PSCs exhibit superior performance [18–21]. This is because the presence of excess iodide can significantly decrease the concentration of halide vacancies, thus serving as a critical factor in achieving higher PCE in PSCs [22]. Furthermore, the presence of surplus iodide ions has the potential to alleviate deep energy level defects within the perovskite layer and reduce iodine vacancies at the ETL/perovskite interface, leading to an enhancement of the V_{OC} [23–26]. Given the mechanism by which iodine enrichment improves PSC performance [12], it can be inferred that, in iodine-rich PSCs, further increases in V_{OC} via reverse-biasing may be limited due to the suppression of iodine vacancies by excess iodine atoms. Therefore, it is imperative to explore the effects of reverse bias on the performance of iodine-rich PSCs.

In this study, we fabricated iodine-rich PSCs, applied reverse bias, compared the photovoltaic parameters of the devices after reverse-biasing with those of control samples, and investigated the mechanisms by which reverse-biasing contributes to performance enhancement. A 3.9% enhancement in short-circuit current density (J_{SC}) is obtained after a reverse-biasing under -0.3 V lasting 2 min. This enhancement is attributed to an improved external quantum efficiency (EQE) in short-wavelength region. The electrochemical impedance spectroscopy (EIS) demonstrated that the trap-states near the ETL/perovskite interface are effectively passivated, and the underlying reason should be related to the directional iodine ion migration to the ETL/perovskite interface, as evidenced by the enhanced I 3d peak in X-ray photoelectron spectroscopy (XPS). These findings provide valuable insights that may inform guidelines for the development of PSCs with higher PCE.

2 | Results and Discussion

2.1 | Improved Performance after Reverse-Biasing

Formal PSCs with layer sequence of fluoro tin oxide (FTO)/TiO₂/FAPbI₃/2,2',7,7'-tetrakis[*N,N*-di(4-methoxyphenyl)amino]–9,9'-spirobifluorene (Spiro-OMeTAD)/Au were fabricated using a two-step process. The research of Yang and You et al. has demonstrated that iodine-rich perovskites can be synthesized by incorporating an adequate quantity of PbI₂ into the precursor solution preparation [26, 27]. Excess PbI₂ has been shown to generate I-type bands within the bulk and at the grain boundaries of perovskite films, which subsequently diminishes the concentration of iodine vacancies and enhances passivation effects. We employed the same experimental methodology as You et al. [27] ensuring the addition of a sufficient amount of PbI₂ in the first step to guarantee that the cells utilized in the reverse bias were iodine-rich. The fabricated PSCs have a typical planar heterojunction structure (Figure 1a).

The baseline photovoltaic current density versus voltage (J – V) curves of the stabilized PSCs were first measured prior to applying reverse bias, with a total of 20 devices tested. The majority of the devices exhibit a PCE of around 22.5% (Figure S1, Supporting Information). The physical diagram and J – V curve of a representative PSC (PCE = 22.61%, V_{OC} = 1.134 V, J_{SC} = 25.80 mA/cm², and FF = 77.26%) are shown in Figure 1b.

After the initial measurements, the 20 samples were evenly divided into five groups. The first served as the control, without reverse-biasing treatment, while the remaining four groups were subjected to reverse-biasing voltages (U_{rb}) of -0.1 , -0.2 , -0.3 , and -0.4 V, respectively, in a dark environment. The control group of devices was used to eliminate the natural performance enhancement of PSCs [28, 29]. Figure 1c presents a comparison of the J – V curves for the PSC at the initial measurement and after being left for 36 h. It can be observed that the performance of the PSC after 36 h, with PCE = 22.44%, V_{OC} = 1.134 V, J_{SC} = 25.82 mA/cm², and FF = 76.59%, shows no obvious difference from the initial values.

The reverse-biasing treatment for each sample lasted 2 min, during which the dark current density (J_{dark}) was continuously monitored. To assess the effect of reverse bias on device performance, five J – V scans were performed at intervals of 0, 1 min, 12, 24, and 36 h after reverse-biasing (Figure 1d). It can be observed that the V_{OC} of the cells measured at different times following the application of reverse bias exhibits no significant change compared to the case without reverse-biasing, which contrasts sharply with the 5% enhancement reported in the existing literature [12]. Figure S2 illustrates the impact of reverse bias on the V_{OC} of low-iodine perovskites. The statistical analysis, as illustrated in Figure 1e,f, indicates that under different reverse bias treatment conditions, there was no significant increase in the V_{OC} and FF. This lack of enhancement can be attributed to the underlying mechanism whereby reverse-biasing promotes the migration of iodide ions, which subsequently occupy iodine vacancies at the interface, thereby enhancing the built-in electric field. However, the PSCs examined in this study are characterized by an iodine-rich composition, resulting in a markedly reduced concentration of iodine vacancies.

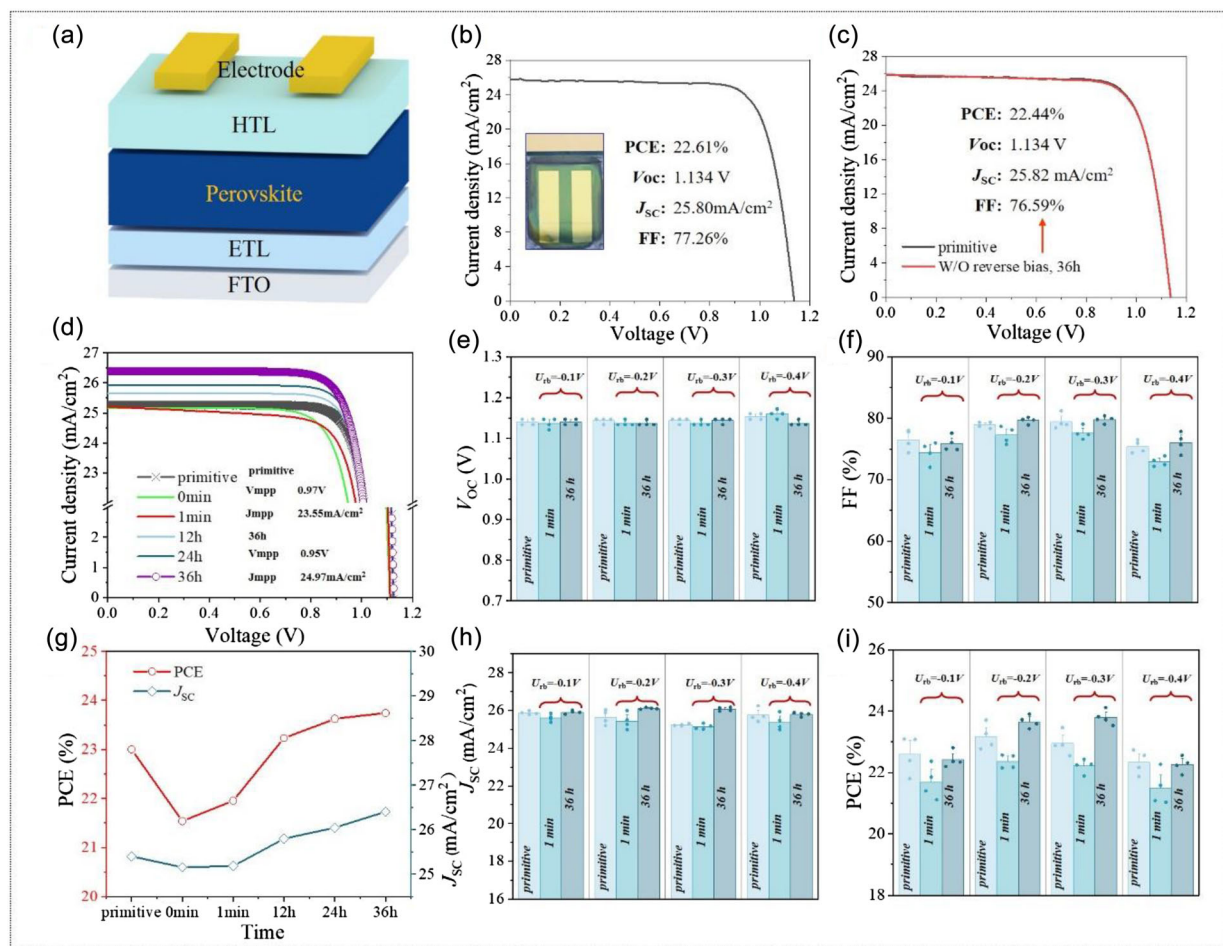


FIGURE 1 | (a) PSCs with FTO/TiO₂/Perovskite/Spiro-OMeTAD/Au planar heterojunction structure. (b) Physical, J - V curves, and electrical characteristic parameters of representative PSCs. (c) Control group: J - V curves of PSCs in the primitive state and after 36 h of storage. (d) J - V curves of PSCs at different times after reverse-biasing processing of -0.3 V. Spectra of (e) V_{OC} , (f) FF, (h) J_{SC} , and (i) PCE under different reverse-biasing voltages. (g) PCE and J_{SC} of a PSC after reverse-biasing at -0.3 V at the different storage time.

Interestingly, in the context of iodine-rich conditions, reverse bias leads to a significant enhancement in the J_{SC} . As shown in Figure 1d, when a reverse bias of -0.3 V is implemented, there is an initial decline in the J_{SC} immediately after the treatment. However, this current progressively increases over time and eventually reaches a stable state. This phenomenon can be attributed to the reorganization of iodide ions to their original positions [12, 30]. A possible process is as follows: During the reverse bias treatment, some I^- ions migrate to the ETL/perovskite interface. These migrated I^- ions can act as a tunneling barrier. When we test the PCE of device at a very short interval, such as 1 min, this tunneling barrier hinders the extraction of photocurrent, resulting in a decrease in efficiency after 1 min. After a longer interval, most of the I^- ions accumulate at the interface and gradually diffuse back into the bulk phase, which reduces the interface barrier. At the same time, some I^- ions remain at the interface, playing a role in modifying the interface. Therefore, when we test the PCE after a longer period, like 36 h, the tunneling barrier that obstructed the photocurrent extraction is no longer present, and the interface recombination is reduced, thus improving the device performance. Once stabilization occurs, the J_{SC} exhibits a notable increase from 25.40 to 26.40 mA/cm², reflecting a 3.9% enhancement. The steady-state output of the device at the maximum

power point after reverse bias treatment is characterized by a voltage of $V_{mpp} = 0.95$ V and a current density of $J_{mpp} = 24.97$ mA/cm². This observation is not an isolated incident: all four cells within the experimental group subjected to a reverse bias of -0.3 V demonstrate a similar upward trend in J_{SC} (Figure 1h), with increases of 3.9%, 2.9%, 3.6%, and 2.4%, respectively.

As a comprehensive result, the PCE of the device shows a significant improvement, increasing from 23.00% to 23.74%, representing a 3.2% enhancement (Figure 1g,i). The figures further demonstrate that PCE rises with the measurement time interval, attributable to the gradual stabilization of the device.

Figure 1e,f,h,i further illustrates the enhancement effect of different reverse bias voltages on performance of PSCs. The application of electric bias facilitates ion migration, allowing halide ions to move toward the ETL and the extent of halide ion migration is related to the magnitude of the reverse bias voltage [31]. When the reverse bias voltages are too small, the electric field may be insufficient to drive the iodide ions to overcome the structural potential barrier, thereby failing to effectively passivate the trap-states. For instance, the samples treated with a -0.1 V reverse bias showed that the PCE, J_{SC} , and V_{OC} were almost

unaffected. Conversely, when the reverse bias voltage is relatively high, some ions may migrate into new potential barriers, creating new defect states. A higher voltage (exceeding -1 V) during reverse bias treatment could also lead to phase segregation induced by ion migration and the formation of parallel shunt currents due to the migration of metal electrodes [12, 32].

2.2 | Enhanced EQE

In order to reveal the underlying mechanism of the change in the performance of PSCs caused by reverse bias, we performed a series of characterization tests on the optical and electrical properties of PSCs before and after reverse-biasing.

The enhancement in J_{SC} can be directly reflected by comparing the EQE of PSCs before and after reverse-biasing. As shown in Figure 2a, the EQE of the PSC after reverse-biasing shows a significant increase in the high-frequency band (300–450 nm) and a small increase in the low-frequency band (around 750 nm). The integrated J_{SC} for the device without reverse bias is 23.84 mA/cm², while the device after reverse bias is 24.51 mA/cm². According to the typical formal planar heterojunction structure in Figure 1a, the high-frequency light is primarily absorbed near the ETL/perovskite interface. As a result, the significant enhancement in EQE within the high-frequency spectrum indicates that the density of trap-state at the ETL/perovskite interface has been effectively mitigated during the reverse-biasing, leading to a substantial decrease in the rate of carrier recombination. To further confirm this conclusion, we have also fabricated inverted perovskite solar cells and applied a reverse bias. A more significant increase in the low-frequency band (650–800 nm) of its

EQE is obtained (Figure S3, Supporting Information). This inference can be substantiated by the characterization outcomes obtained from EIS (Figure 2b). The asymmetrical semicircle in the low-frequency region corresponds to the composite resistance (R_{re}), which is significantly increased from 5.973×10^4 to 4.783×10^5 ohm cm⁻² after reverse-biasing, indicating that the recombination of the carriers within the PSC is significantly suppressed. Conversely, the small semicircle in the high-frequency region corresponds to the charge transfer resistance (R_{ct}) at the interface, which reduced from 4.488×10^5 to 5.557×10^4 ohm cm⁻² after reverse-biasing, indicating a better carrier collection, thereby contributing to the elevated EQE in the high-frequency band [12, 33–35]. The slight increase in EQE of PSCs after reverse-biasing in the low-frequency band can also be attributed to the suppressed recombination of carriers, as evidenced by the increased R_{re} .

Furthermore, the reverse bias has little effect on the lattice structure and optical properties of perovskite materials. Figure 2c compares the UV–vis absorption spectroscopy of the perovskite layer before and after reverse-biasing. It can be observed that, the perovskite layer exhibits comparable light absorption ability before and after reverse-biasing, which indicates that the reverse bias does not change the crystal structure and band gap of the material. In addition, the significant increased intensity of the PL peak (Figure 2d), also suggests a decrease in non-radiative recombination, thus indicating a reduction in defect states in PSCs after reverse-biasing [31].

The hardly increased V_{OC} for the reverse bias treated PSCs can be mainly attributed to the excess iodine. In this case, the iodine vacancies in the PSCs are minimal [22–27], which implies that the iodine ions, driven toward the ETL/perovskite interface

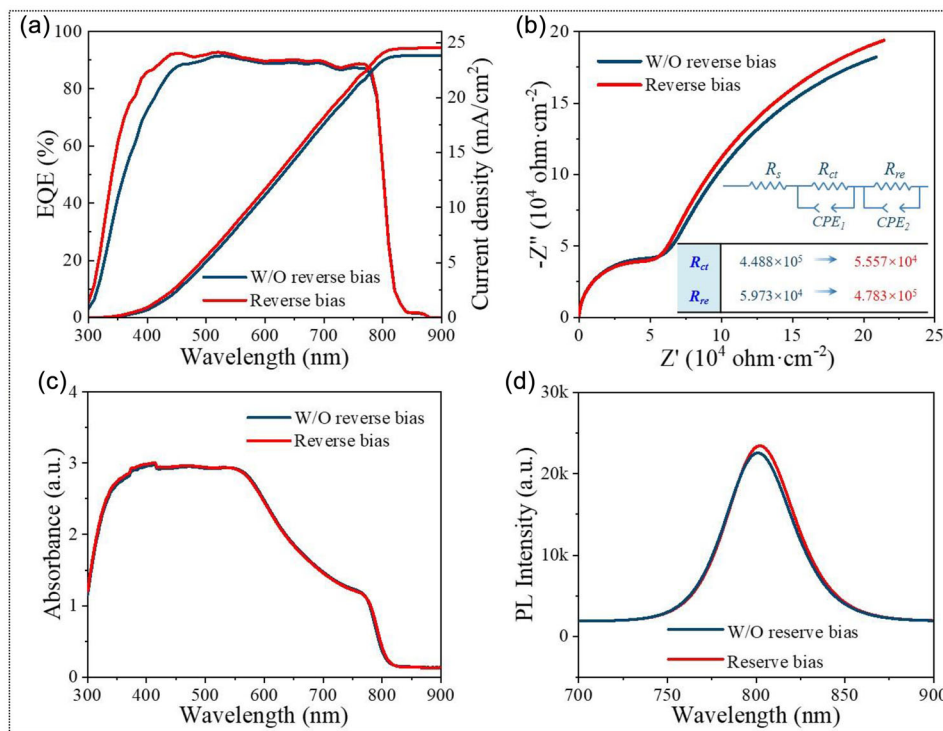


FIGURE 2 | (a) EQE of pre- and post-back-biased PSCs, the right axis is the J_{SC} calculated by the overlap integration of the EQE spectrum with the standard AM1.5G. (b) EIS plots of PSCs before and after reverse-biasing. (c) UV–vis curves of PSCs before and after reverse-biasing. (d) PL curves of PSCs before and after reverse-biasing.

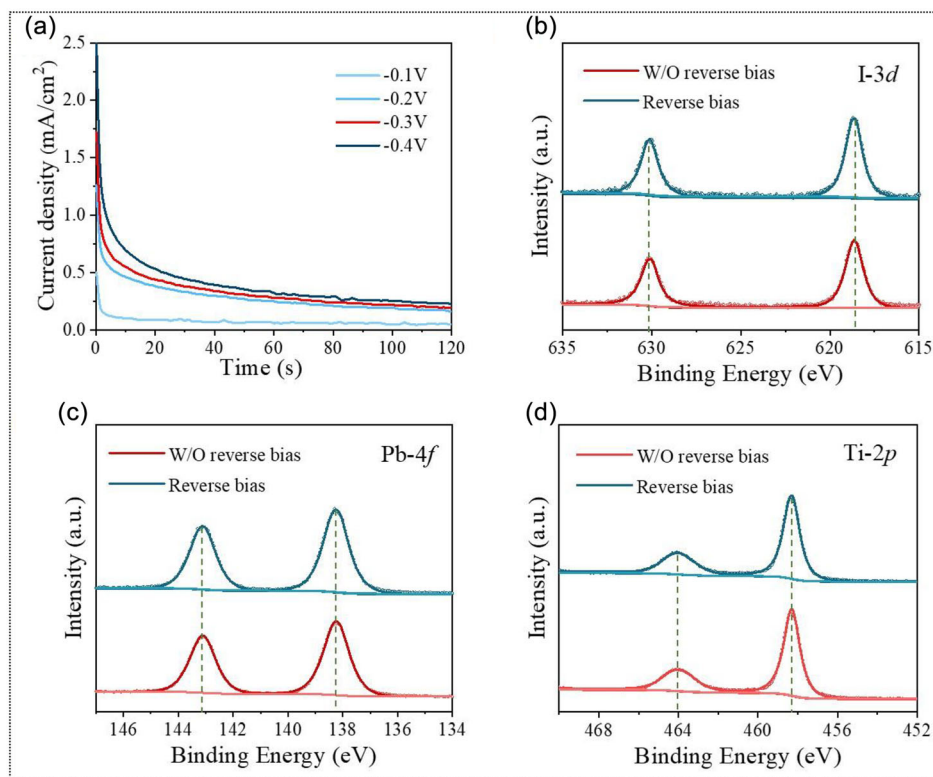


FIGURE 3 | (a) Dark current density of PSCs monitored during reverse-biasing treatments. XPS spectra of (b) I 3d, (c) Pb 4f, and (d) Ti 2p of TiO₂.

due to reverse-biasing, cannot be effectively accommodated by a sufficient number of iodine vacancies. Consequently, the majority of these iodine ions that accumulate at the interface are likely to revert to their original positions. As illustrated in Figure 1e, when subjected to a relatively high voltage of -0.4 V, the V_{OC} increases after reverse-biasing treatment for 1 min; however, after 36 h, the increase disappears and even decreases. This decreased V_{OC} can be attributed to phase segregation induced by ion migration at elevated voltages [12].

2.3 | Directional Iodine Ions Migration under Reverse-Biasing

Iodine ion migration in PSCs during and subsequent to the reverse bias treatment should be the fundamental reason that affects the performance of the PSCs. During the reverse bias treatment process, we monitored the temporal changes in dark current, with the results shown in Figure 3a. The data reveal that during the reverse bias treatment process, the reverse current increases rapidly on a timescale of less than 1 s, which corresponds to the response of electrons and holes to the reverse voltage. This is followed by a gradual decrease, ultimately stabilizing over a period of about 100 s, which is associated with ion migration in the PSCs. Both electronic and ionic currents are observed to rise with increasing reverse voltage, attributable to the enhanced electric field.

Upon migration to the ETL/perovskite interface, the iodine ions tend to accumulate at the interface, which can be confirmed by the XPS spectra of the TiO₂ layers before and after reverse-biasing (Figure 3b). To obtain the TiO₂ layer for characterization,

DMF was used to dissolve the upper perovskite layer. The results show that the intensity of I 3d peaks in the TiO₂ film after reverse-biasing is greater than that of the control sample. While, the differences in the intensities of Pb 4f and Ti 2p peaks (Figure 3c,d) between the control and reverse bias sample are negligible. These two pieces of information together indicate that the enhanced I 3d peaks are not from the residual lead iodide at the interface, thus providing direct evidence for the directional migration of iodine ions to and their accumulation at the ETL/perovskite interface, under the electric field induced by reverse-biasing. Furthermore, there was no shift in the peak locations of I 3d and Ti 2p after reverse-biasing treatment, indicating that such treatment does not facilitate the formation of new I-Ti bonds in iodine-rich scenarios characterized by a scarcity of iodine vacancies. The XPS spectra for other elements, including C, N, and O, exhibit minimal changes post-reverse-biasing (Figure S4, Supporting Information).

3 | Conclusions

We have elucidated the impact of reverse bias on the performance of iodine-rich PSCs. After a reverse-biasing under a -0.3 V voltage for 2 min, the J_{SC} of the PSCs initially experiences a decline, subsequently increasing and stabilizing after 36 h. The J_{SC} of such treated PSCs can be improved by $\approx 3.9\%$, from 25.40 to 26.40 mA/cm². This improvement is primarily attributed to the effective passivation of trap-states at the ETL/perovskite interface by iodine ions migrating under reverse-biasing. This is supported by the increased R_{re} and the reduced interfacial R_{ct} of the PSCs, both of which result in an enhanced EQE in the high-frequency band corresponding to the region near the ETL/perovskite

interface. Additionally, the reduction of non-radiative recombination of perovskites, as evidenced by the PL spectra, also contributes to the enhancement of J_{SC} . The V_{OC} shows insignificant changes under reverse-biasing, which is attributed to the iodine-rich nature of the PSCs. In this context, the iodine ions, influenced by the electric field, migrate toward the ETL/perovskite interface but do not achieve stability, thereby failing to significantly enhance the built-in electric field. As a comprehensive effect, the PCE of PSCs after reverse-biasing improves by $\approx 3.2\%$, from 23.00% to 23.74%. The directional migration of iodine ions to the ETL/perovskite interface under reverse-biasing is evidenced by the enhanced intensity of I 3d peak at the ETL/perovskite interface. We anticipate that further clarifications of the effects of reverse bias will enable the development of guidelines for achieving higher-efficiency devices with enhanced stability.

4 | Experimental Section

4.1 | Device Fabrication

Formal PSCs using a perovskite thin film with the composition $FAPbI_3$ were fabricated in an inert atmosphere (N_2 -filled glovebox). Initially, the $1.2 \times 1.8 \text{ cm}^2$ glass substrates with a 500 nm thick FTO coating (sheet resistance 8Ω , provided by SJNYO Co., Ltd.) were cleaned in an ultrasonic bath sequentially with glass water, ultrapure water, and ethanol and ultrapure water, spending 15 min for each step. Then, the substrates were treated by an ultraviolet ozone for 20 min (UV, LEBO Science UC100-SE). Next, the FTO glasses were immersed in a 2.2% $TiCl_4$ aqueous solution, a heating in a water bath at a constant temperature of 70°C for 35 min to synthesis the TiO_2 ETL and a

UV ozone treatment for 15 min to modify the interface. The $FAPbI_3$ thin films were spin-coated on the top of the TiO_2 layer using the same two-step process as You et al. [27] ensuring that the resulting devices were all iodine-rich, which is an adequate concentration commonly utilized in the synthesis of iodine-rich perovskites: (1) the precursor solution with 1.5 M PbI_2 (a sufficient amount) and 0.045 M $RbCl$ in DMF:DMSO (volume ratio = 9:1) mixed solvent was prepared, spin-coated on TiO_2 layer at 1500 rpm for 30 s and then annealed at 70°C for 65 s; (2) the FAI solution (90 mg:13 mg, 1 mL isopropanol) was spin-coated at 1800 rpm for 30 s, followed by annealing at 40°C for 60 s; (3) further annealing was conducted at 130°C in an air environment (40% relative humidity) for 15 min to obtain the stable iodine-rich cubic phase perovskite layers. Next, a PEAI layer was prepared by spin-coating PEAI solution (4.5 mg, 1 mL isopropanol) on the perovskite at 4000 rpm for 30 s, to passivate and protect the perovskite film. Subsequently, the HTL layer was fabricated by spin-coating a Spiro-OMeTAD solution at 4000 rpm for 30 s. The Spiro-OMeTAD solution was prepared by dissolving 72.3 mg of Spiro-OMeTAD and 28.6 μL of 4-tert-butylpyridine in 1 mL of chlorobenzene, with the addition of 17.5 μL of lithium bis (trifluoromethanesulfonyl) imide solution in acetonitrile (520 mg mL^{-1}). Finally, Au electrode with thickness of 50–60 nm was prepared via thermal evaporation. It should be noted that the freshly prepared PSCs should be self-stable by storing them overnight in drying oven with controlled temperature of $23\text{--}25^\circ\text{C}$ and relative humidity of 3%.

4.2 | Reverse-Biasing Experiments

The reverse-biasing experiments were performed using a custom-built platform (Figure 4). A solar simulator (CME-sol8100-AAB,

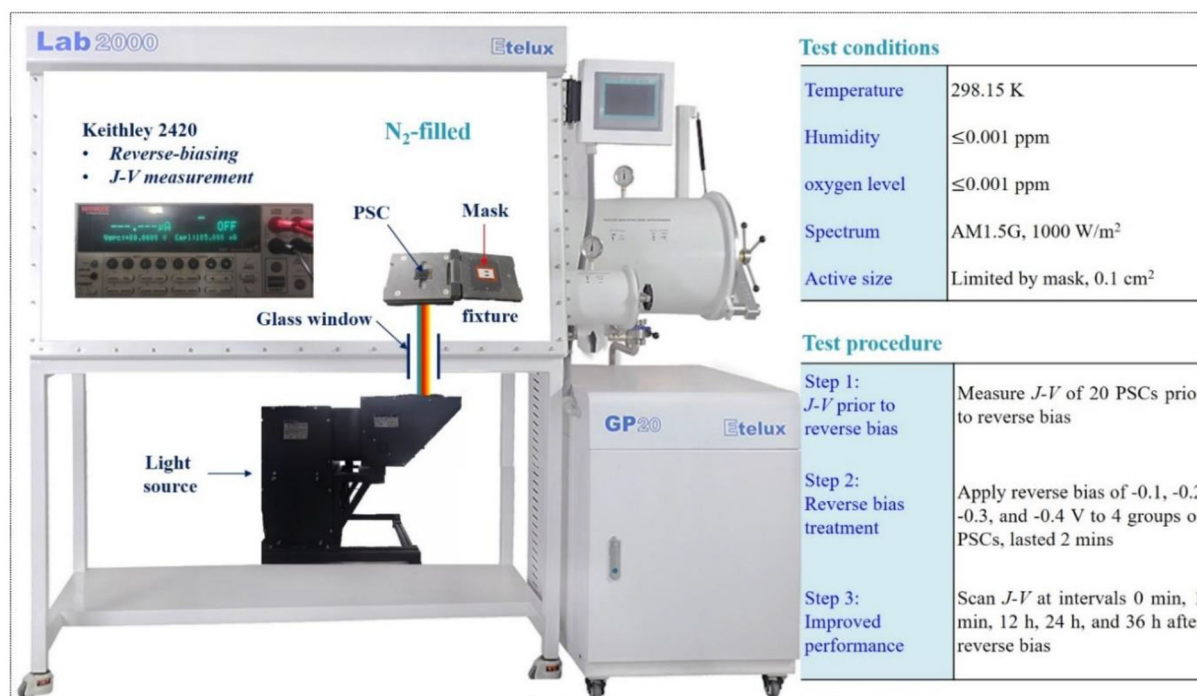


FIGURE 4 | Illustration of the custom-built platform used for the reverse-biasing experiments, along with the corresponding test conditions and procedures.

microenerg) was positioned beneath a glovebox equipped with a glass window in its bottom plate. This design allowed light to pass through the window and illuminate the PSC, which was fixed on the test fixture, from below. A Keithley 2420 source meter was utilized to apply reverse bias to the PSCs and measure their J - V curves. All experiments were conducted in an N_2 -filled environment at a controlled temperature of 25°C. Humidity and oxygen levels were maintained below 0.001 ppm. The AM 1.5G spectrum, with an effective irradiance of 1000 W/m², was selected to measure the J - V characteristics of the PSCs. During the measurements, the active size of the PSCs was limited to 0.1 cm² by the mask of the test fixture. Between measurements, the devices were stored in a drying oven with controlled temperature of 23–25°C and relative humidity of 3%.

4.3 | Characterizations

UV–vis absorption spectra (UV-2600i, Shimadzu) were measured to compare the light-absorption capability of perovskite layer before and after reverse-biasing. PL spectra (LQ-100X, Enlitech, 405 nm, 120 mW/cm² (100%)) were measured to reveal the emission and the radiative recombination in the perovskite layer. We conducted PL measurements using a top-illumination vertical configuration, where a 405 nm laser was vertically incident from a position 5–10 mm above the top, and the reflected PL signal was detected. EQE (QE-R, Enlitech) was measured to observe PSCs' behavior in a specific range of wavelength and reflect the comprehensive effects of reverse bias on the light absorption, carrier recombination, and carrier collection efficiency of PSCs. EIS (IM3570 HIOKI) was measured to investigate carrier dynamics, which can reveal the composite resistance and charge transfer resistance in PSCs. XPS (Nexsa G2, Thermo Scientific) was used to characterize elemental changes on the TiO₂ films after reverse-biasing to evidence the migration of iodine ions.

Acknowledgments

This work is supported partially by the National Natural Science Foundation of China (grant nos. 52072121, 52232008, 51972110, 52102245, 52402254, and 22409061), Beijing Natural Science Foundation (Z240024, 2222076, and 2222077), 2022 Strategic Research Key Project of Science and Technology Commission of the Ministry of Education, Huaneng Group Headquarters Science and Technology Project (HNKJ20-H88), State Key Laboratory of Alternate Electrical Power System with Renewable Energy Sources (LAPS2024–05), the Fundamental Research Funds for the Central Universities (2022MS029, 2022MS02, 2022MS031, and 2023MS042, 2023MS047), and the NCEPU “Double First-Class” Program.

Conflicts of Interest

The authors declare no conflicts of interest.

Data Availability Statement

The data that support the findings of this study are available from the corresponding author upon reasonable request.

References

1. M. A. Green, E. D. Dunlop, M. Yoshita, et al., *Progress in Photovoltaics: Research and Applications* 32 (2024): 425–441.

2. S. Li, Y. Jiang, J. Xu, et al., *Nature* 635 (2024): 82–88.
3. H. Wang, Y. Zheng, G. Zhang, et al., *Advanced Materials* 36 (2024): 2307855.
4. L. Yang, J. Feng, Z. Liu, et al., *Advanced Materials* 34 (2022): 2201681.
5. X. Zhao, Y. Qiu, M. Wang, et al., *ACS Energy Letters* 9 (2024): 2659–2669.
6. Q. Zhang, H. Huang, Y. Yang, et al., *Advanced Materials* 36 (2024): 2410390.
7. H. Huang, P. Cui, Y. Chen, et al., *Joule* 6 (2022): 2186–2202.
8. Y. Wang, L. Li, Z. Wu, et al., *Angewandte Chemie International Edition* 62 (2023): e202302342.
9. T. Wu, P. Wang, L. Zheng, Y. Zhao, and Y. Hua, *Advanced Energy Materials* 14 (2024): 2400078.
10. L. Yan, H. Huang, P. Cui, et al., *Nature Energy* 8 (2023): 1158–1167.
11. P. Cui, D. Wei, J. Ji, et al., *Nature Energy* 4 (2019): 150–159.
12. K. Huang, X. Feng, H. Li, et al., *Advanced Science* 9 (2022): 2204163.
13. J. Wu, Y. Li, S. Tan, et al., *ACS Applied Materials & Interfaces* 12 (2020): 27258–27267.
14. K. Jeong, J. Byeon, J. Jang, N. Ahn, and M. Choi, *Joule* 6 (2022): 1087–1102.
15. Z. Ni, H. Jiao, C. Fei, et al., *Nature Energy* 7 (2022): 65–73.
16. L. Bertoluzzi, J. B. Patel, K. A. Bush, et al., *Advanced Energy Materials* 11 (2021): 2002614.
17. C. Wang, L. Huang, Y. Zhou, et al., *Advanced Energy Materials* 13 (2023): 2203596.
18. Q. Tian, G. Ding, Y. Cai, et al., *ACS Applied Energy Materials* 4 (2021): 7535–7543.
19. S. Ma, X. Xue, K. Wang, et al., *Advanced Energy Materials* 14 (2024): 2303193.
20. S. Ullah, P. Yang, J. Wang, et al., *Physica Status Solidi A* 218 (2021): 2100271.
21. J. Hu, J. W. Ahn, Z. Xu, et al., *Advanced Energy Materials* 14 (2024): 2400500.
22. B. Park, N. Kedem, M. Kulbak, et al., *Nature Communications* 9 (2018): 3301.
23. W. S. Yang, B. Park, E. H. Jung, et al., *Science* 356 (2017): 1376–1379.
24. S. Mahesh, J. M. Ball, R. D. Oliver, et al., *Energy and Environmental Science* 13 (2020): 258–267.
25. J. He, W. Fang, and R. Long, *Chemical Science* 10 (2019): 10079–10088.
26. Q. Chen, H. Zhou, T. Song, et al., *Nano Letters* 14 (2014): 4158–4163.
27. Y. Zhao, F. Ma, Z. Qu, et al., *Science* 377 (2022): 531–534.
28. Y. Cho, H. D. Kim, J. Zheng, et al., *ACS Energy Letters* 6 (2021): 925–933.
29. S. Moghadamzadeh, I. M. Hossain, M. Jakoby, et al., *Journal of Materials Chemistry A* 8 (2020): 670–682.
30. W. Li, K. Huang, J. Chang, et al., *ChemPhysMater* 1 (2022): 71–76.
31. L. Li, P. Jia, W. Bi, et al., *Rsc Advances* 10 (2020): 28083–28089.
32. R. A. Razera, D. A. Jacobs, F. Fu, et al., *Journal of Materials Chemistry A* 8 (2020): 242–250.

33. Y. Yang, H. Huang, L. Yan, et al., *Advanced Energy Materials* (2024): 2400416.
34. H. Zarenezhad, M. Askari, M. Halali, N. Solati, T. Balkan, and S. Kaya, *Sol. Energy Mater. Sol. Cells* 206 (2020): 110318.
35. C. Sun, Y. Guo, H. Duan, et al., *Sol. Energy Mater. Sol. Cells* 143 (2015): 360–368.

Supporting Information

Additional supporting information can be found online in the Supporting Information section.